

On the SRT – MRT Lattice Boltzmann Method: Validity Limits of the Single Relaxation Time for Simulating Single-Phase Flows

Ameer K. Alhilo, Wessam F. Hasan, and Hassan Farhat

Abstract—The multi-relaxation time (MRT) Lattice Boltzmann method (LBM) was developed to overcome several constraints, which are inherent to the more famous single relaxation time (SRT) Bhatnagar–Gross–Krook (LBGK) model. Constraints, such as fixed Prandtl number, fixed ratio between kinematic and bulk viscosity, and Reynolds number limitations undermine the SRT usefulness. Furthermore, the SRT method fails to accurately characterize high viscosity fluids' behavior near the domain's walls, an issue which can be circumvented with the MRT method. However, the MRT requires a careful selection of its relaxation parameters for achieving the desired outcome. The ad-hoc nature of this selection makes the method cumbersome, especially for three-dimensional (3D) domains. Additionally, it is known that the MRT solution requires about 10% - 15% more computational time than the SRT for the same domain size.

Four widely used single-phase flow conditions were explored by using the SRT and the MRT methods. It is shown that the SRT has good accuracy when used for simulating low viscosity fluid cases; however, the SRT exhibits a non-physical velocity jump at the domain surface boundaries when used for simulating high viscosity fluid flows. This issue can be resolved by augmenting the SRT domain's height, which in turn leads to an increase in the required computational time. The main advantages of the MRT are due to its capability in overcoming the velocity jump in most of the high viscosity fluid cases and in its ability to simulate flows with ultra-low viscosities, which was demonstrated in the characterization of the flow around S822 airfoil with Reynolds number $Re \approx 40,000$.

Index Terms—Lattice boltzmann, multi-relaxation time LBM, LBGK, parabolic flow, S822 airfoil, drag and lift.

I. INTRODUCTION

The MRT LBM was introduced by D'Humières [1] to overcome defects inherent to the Lattice gases, which suffered from important statistical noise due to averaging Boolean variables for calculating the macroscopic variables. At the time, when several researchers simulated the motion of particles by their occupation number rather than their Boolean occurrence and used a relaxation process towards equilibrium prescribed by the kinetic theory, D'Humières suggested the addition of new degrees of freedom for the choice of equilibrium distribution.

Since its inception, the MRT LBM presented an interesting simulation platform, which attracted the attention of several researchers, who tried to analyze, further develop and use it for simulation cases, which were inaccessible to the SRT LBM users. Lallemand and Lue [2] obtained a generalized hydrodynamics (wave vector dependence of the transport coefficient) by solving the dispersion equation of the linearized lattice Boltzmann equation either analytically or numerically. The authors applied the concept for selecting the adjustable parameters to optimize dispersion, dissipation, anisotropy and the Galilean invariance of their model. The generalized hydrodynamics was used to study the stability of two-dimensional shear flow with shock, in which the simulation results matched their theoretical analysis. D'Humières *et al.* [3], extended the MRT method to D3Q15 and D3Q19 three-dimensional domain, to simulate lid-driven cavity flow for Reynolds numbers up to $Re = 2000$. J.-S. Wu, Y.-L. Shao [4] simulated two-dimensional near-incompressible steady lid-driven cavity flows with Reynolds number between 100 and 7500 by using MRT and LBGK models. The results were compared with Navier-Stokes simulation results for the same flow domain and flow conditions. The authors reported that the MRT was able to improve the solution convergence, to decrease the spatial oscillations near sharp edges as well as it was successful in simulating high Reynolds number cases. The improvements were due to the different relaxation rates used for different physical modes, which were embedded in the MRT scheme. Rui *et al.* [5] proposed an incompressible MRT LBM, with the equilibria in momentum space were derived from a previous LBGK model for incompressible flow proposed by Guo *et al.* [6]. The Model was successfully applied to steady state Poiseuille flow, cavity driven flow and double shear flow in 2D domains. Jafari S. and Rahnama M. [7] used the generalized lattice Boltzmann equation for the computation of turbulent channel flow and compared successfully their results for mean velocity distribution, turbulent statistics and vortical structures with the large eddy simulation with shear-improved Smagorinsky model for the subgrid-scale turbulence effects. The model showed good numerical stability and ease in parallelization. E. Aslan *et al.* [8] studied the classical case of the two-dimensional lid cavity for incompressible steady laminar flow using the SRT and the MRT methods. For high Reynolds numbers ranging between 200 and 2000, the results were compared with the finite-volume predictions of the incompressible Navier-Stokes equations. The MRT showed more stable results than the SRT for high Reynolds numbers. The authors compared the convergence speed between MRT and SRT within the stability range, and they

Manuscript received November 18, 2019; revised May 3, 2020.

Ameer K. Alhilo is with Wayne State University, Detroit, MI, USA and Wasit University, Kut, Iraq.

Wessam F. Hasan is with North Oil Company, Kirkuk, Iraq.

Hassan Farhat is with Wayne State University, Detroit, MI, USA (e-mail: av9328@wayne.edu).

found that the LBM- SRT was about 10% faster than the MRT and that both simulation time were greater than the general-purpose finite-volume based CFD code. Suga *et al.* [9] developed a D3Q29 for the simulation of turbulence in fully developed channel, pipe and porous media with round wall boundaries for the latest two. The model results correlated well with the results of direct and large simulations.

Furthermore, the MRT method was successfully used in the study of calculation of friction coefficient and analysis of fluid flow in a stepped micro-channel for wide range of Knudsen number [10]. Same method was employed in the study of soli-liquid phase change [11], mixing in an active micromixer with rotationally oscillating stirrer in high Peclet number flows [12], for investigating of three dimensional MHD natural convection [13] and for simulating laminar and transition flows in natural convection cases [14].

Several LBM airfoil studies were published in recent years. Among them is the work of Imamura *et al* [15], who extended the LBM algorithm to generalized coordinates. The authors results matched very well those from CFL3D. The model was combined with the Baldwin-Lomax turbulence model for improved results for high Reynolds numbers. Imamura *et al.* [16] applied the local time step method on non-uniform grid to simulate flow around airfoil in order to validate the code with the local time step method. The authors' results for pressure distribution and aerodynamic coefficients were consistent with previous study. Imamura *et al.* claimed a reduction of 70-80% of CPU time compared to solutions with global time step.

Rajani *et al.*, [17] utilized LBM based very large eddy simulation approach, to simulate the flow around semi-span NACA0012 airfoil with rounded tip. Their results for mean pressure coefficient, mean velocity field distribution and the location of the vortex core agreed with experimental data. Rajanial, [18] studied the time averaged mean flow fields for multi-element airfoil with several attack angles around the slat cove and compared successfully their simulation outcome with experimental data and a Navier-Stokes based numerical solution.

Xiao-Peng Chen [19], who used MRT-LBM scheme coupled with the Spalart-Allmaras turbulence model to simulate the two-dimensional turbulent flow around NACA0012 airfoil, with $Re=10^5$ and angle of attack $\alpha = 4^\circ$. Xiao-Peng Chen refined the mesh around the airfoil and used the no-slip boundary condition at the lower and upper boundaries, the non-equilibrium extrapolated method for constant velocity and pressure conditions at the inlet and outlet boundaries, respectively. Chen validated his model via a direct comparison with the SST and the SST- γ - $Re\theta$ model by Council and Boulama [20]. The model was able to capture the flow separation, which was indicated in the pressure coefficient on the airfoil surface, while maintaining a small difference in predicting the C_p value in the flow separation region.

Amin Poozesh and Masoud Mirzaei [21], used the interpolation lattice Boltzmann method for simulating the unsteady fluid flow around a cambered airfoil in a non-uniform grid. The author's used the SRT-LBM with adaptive mesh generation for the study of incompressible viscous flow around a cambered airfoil for a range of angles

of attack $\alpha = 0 - 15$ and low Reynold number $Re = 1000$ with free stream velocity of 0.1 m/s. The Strouhal number, the pressure, the drag and the lift coefficients, which were obtained from the simulations agreed well with classical computational fluid dynamics simulations. The main advantages of this simulation method were the ability to choose complex geometry, to predict the vortex behind a vertical plate symmetrical and non-symmetrical at high angles of attack and finally exploit the power of parallel computing.

Prabhukhot P. and Prabukhot A. [22] used ANSYS fluent to study the behavior of S822/S823 blade profile at various contours and reported a maximum turbulence and minimum pressure near the trailing edge of the blade's tip.

In this work, the MRT and SRT methods are implemented for simulating fluid flows under very useful conditions such as simple shear flow, uniaxial extensional flow, flow between two parallel plates with velocity inlet and extrapolation outlet boundary conditions and two parallel plates' flow with constant source term (pressure drop per unit length). This is to provide users' guidance for selecting the most optimal approach for the simulation problem in question and to avoid the generalization that the SRT is exclusively inferior and inaccurate as compared to the MRT. The validation of the basic cases is done through a comparison with available theoretical solutions.

Additionally, it is shown that the MRT method can be used to calculate the lift and drag coefficients for S822 airfoil for attack angle of 5.25 degree and Reynolds number $Re \approx 40,000$. The coefficients are computed via a simplistic approach, which does not require irregular mesh and data extrapolation. The MRT results agree well with the results of Xfoil [25] using turbulence index $Ncrit = 5$.

II. NUMERICAL METHOD

A. LBGK Model

The single relaxation Bhatnagar-Gross- Krook (BGK) lattice Boltzmann (LBM), single-relaxation model used in this work, is based on the Boltzmann kinetic equation:

$$\frac{df}{dt} + \xi \cdot \nabla f = -\frac{1}{\lambda}(f - f^{eq}) \quad (1)$$

where f is the density distribution function, ξ is the macroscopic velocity, f^{eq} is the equilibrium distribution function, and λ is the physical relaxation time. Equation (1) is first discretized by using a set of velocities $\{\xi_i\}$ confined to a finite number of directions and this leads to the following equation:

$$\frac{df_i}{dt} + \xi_i \cdot \nabla f_i = -\frac{1}{\lambda}(f_i - f_i^{eq}) \quad (2)$$

The lattice links for the D2Q9 BGK used in this work are shown in Fig. 1. These links have the following endpoints coordinates:

$$\begin{aligned} &c_0(0,0); c_1(1,0); c_2(0,1); c_3(-1,0); c_4(0,-1); \\ &c_5(1,1); c_6(-1,1); c_7(-1,-1); c_8(1,-1) \end{aligned} \quad (3)$$

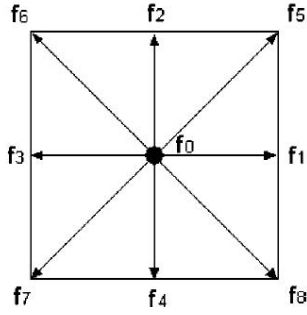


Fig. 1. Velocity vectors for the D2Q9 lattice Boltzmann method used in this model.

In the LBM Eq. (2) is further discretized in the lattice space and time which leads to the following:

$$\hat{f}_i(x, t + \delta_t) = f_i(x, t) - \frac{1}{\tau} [f_i(x, t) - f_i^{eq}(\rho, \rho u)] + \phi_i(x) \quad (4)$$

The lattice space δ_x and the lattice time step δ_t are taken as unity and their ratio $c = \delta_x / \delta_t = 1$. The lattice speed of sound $c_s = c / \sqrt{3}$ is used for determining the fluid pressure by $p = \rho c_s^2$, and the lattice relaxation time is $\tau = \lambda / \delta_t$. The kinematic viscosity is derived from the relaxation time by the following:

$$\nu = (\tau - 0.5) c_s^2 \delta_t \quad (5)$$

The relation between the macroscopic and spatially varying lattice source term, is given by Guo *et al.* [12]:

$$\phi_i(\mathbf{x}) = k_2 \omega_i \left(1 - \frac{1}{2\tau} \right) \left[\frac{\mathbf{c}_i \cdot \mathbf{u}}{c_s^2} + \frac{(\mathbf{c}_i \cdot \mathbf{u}) \mathbf{c}_i}{c_s^4} \right] \cdot \mathbf{F}(\mathbf{x}) \quad (6)$$

where, $k_2 \delta_{\alpha\beta\gamma} = \sum_i \omega_i e_{i\alpha} e_{i\beta} e_{i\gamma}$ and ω_i are weighting constants.

The streaming step is executed by the following equation:

$$f_i(\mathbf{x} + \mathbf{c}_i \delta_t, t + \delta_t) = \hat{f}_i(\mathbf{x}, t + \delta_t) \quad (7)$$

where, $\hat{f}_i(\mathbf{x}, t + \delta_t)$ is the post collision's density distribution function. The macroscopic density and momentum are obtained from the distribution function as follows:

$$\rho = \sum_{i=0}^{Q-1} f_i = \sum_{i=0}^{Q-1} f_i^{eq} \quad (8)$$

$$\rho \mathbf{u} = \sum_{i=1}^{Q-1} \mathbf{c}_i f_i = \sum_{i=1}^{Q-1} \mathbf{c}_i f_i^{eq} \quad (9)$$

B. The MRT Method

The multi-relaxation time (MRT), known as the generalized lattice Boltzmann equation (GLBE) or moment method, helps overcome some of the main constraints of the single relaxation (SRT) or LBGK model. Following the footsteps of D'Humiers *et al* [3], Lallemand and Luo [2] and other, the MRT method is implemented via mapping the population space to moment space and by using the Gram-Schmidt matrix approach for D2Q9:

$$\mathbf{F} = \begin{bmatrix} \rho \\ e \\ \varepsilon \\ j_x \\ q_x \\ j_y \\ q_y \\ p_{xx} \\ p_{xy} \end{bmatrix} = \begin{bmatrix} 1 & 1 & 1 & 1 & 1 & 1 & 1 & 1 & 1 \\ -4 & -1 & 2 & -1 & 2 & -1 & 2 & -1 & 2 \\ 4 & -2 & 1 & -2 & 1 & -2 & 1 & -2 & 1 \\ 0 & 1 & 1 & 0 & -1 & -1 & -1 & 0 & 1 \\ 0 & -2 & 1 & 0 & -1 & 2 & -1 & 0 & 1 \\ 0 & 0 & 1 & 1 & 1 & 0 & -1 & -1 & -1 \\ 0 & 0 & 1 & -2 & 1 & 0 & -1 & 2 & -1 \\ 0 & 1 & 0 & -1 & 0 & 1 & 0 & -1 & 0 \\ 0 & 0 & 1 & 0 & -1 & 0 & 1 & 0 & -1 \end{bmatrix} \begin{bmatrix} f_0 \\ f_1 \\ f_2 \\ f_3 \\ f_4 \\ f_5 \\ f_6 \\ f_7 \\ f_8 \end{bmatrix} = \mathbf{M} \cdot \mathbf{f} \quad (10)$$

where, \mathbf{M} is 9×9 matrix used to transform \mathbf{f} from the discrete space into \mathbf{F} in the moment space. In the column vector \mathbf{F} , ρ is the fluid density, ε is a function of the square of the energy e , j_x and j_y are the mass flux in the horizontal and vertical directions, q_x and q_y are the energy flux in the horizontal and vertical directions, p_{xx} and p_{xy} correspond to the diagonal and the off-diagonal components of the viscous stress tensor.

The equilibrium moment vector can be obtained by $\mathbf{F}^{eq} = \mathbf{M} \mathbf{f}^{eq}$ to a second order in velocity. A more efficient way is to find analytical expressions for the vector elements as functions of the velocity and density:

$$\mathbf{F}^{eq} = \begin{bmatrix} \rho^{eq} = \rho \\ e^{eq} = \rho(-2 + 3(u^2 + v^2)) \\ \varepsilon^{eq} = \rho(1 - 3(u^2 + v^2)) \\ j_x^{eq} = \rho u \\ q_x^{eq} = -\rho u \\ j_y^{eq} = \rho v \\ q_y^{eq} = -\rho v \\ p_{xx}^{eq} = \rho(u^2 - v^2) \\ p_{xy}^{eq} = \rho uv \end{bmatrix} \quad (11)$$

The collision state is executed in the moment space by the following:

$$\mathbf{F}^* = \begin{bmatrix} \rho^* = \rho - s_0(\rho - \rho^{eq}) \\ e^* = e - s_1(e - e^{eq}) \\ \varepsilon^* = \varepsilon - s_2(\varepsilon - \varepsilon^{eq}) \\ j_x^* = j_x - s_3(j_x - j_x^{eq}) \\ q_x^* = q_x - s_4(q_x - q_x^{eq}) \\ j_y^* = j_y - s_5(j_y - j_y^{eq}) \\ q_y^* = q_y - s_6(q_y - q_y^{eq}) \\ p_{xx}^* = p_{xx} - s_7(p_{xx} - p_{xx}^{eq}) \\ p_{xy}^* = p_{xy} - s_8(p_{xy} - p_{xy}^{eq}) \end{bmatrix} = \mathbf{F} - \mathbf{S}(\mathbf{F} - \mathbf{F}^{eq}) \quad (12)$$

The relaxation parameters represent the diagonal elements of the matrix \mathbf{S} :

$$\mathbf{S} = \begin{bmatrix} s_0 & 0 & 0 & 0 & 0 & 0 & 0 & 0 & 0 \\ 0 & s_1 & 0 & 0 & 0 & 0 & 0 & 0 & 0 \\ 0 & 0 & s_2 & 0 & 0 & 0 & 0 & 0 & 0 \\ 0 & 0 & 0 & s_3 & 0 & 0 & 0 & 0 & 0 \\ 0 & 0 & 0 & 0 & s_4 & 0 & 0 & 0 & 0 \\ 0 & 0 & 0 & 0 & 0 & s_5 & 0 & 0 & 0 \\ 0 & 0 & 0 & 0 & 0 & 0 & s_6 & 0 & 0 \\ 0 & 0 & 0 & 0 & 0 & 0 & 0 & s_7 & 0 \\ 0 & 0 & 0 & 0 & 0 & 0 & 0 & 0 & s_8 \end{bmatrix} \quad (13)$$

where s_0, s_3, s_5 are related to the conserved moments of the density and momentum, which are invariant and therefore these parameters values do not matter. The parameter s_1 is related to the bulk viscosity, and $s_7 = s_8 = \frac{1}{\tau}$ determine the shear viscosity. The rest s_2, s_4, s_6 are free parameters used to tune the model. The transformation back from the moment space into the population space is given by:

$$f^* = M^{-1}F^* = f - M^{-1}S[F - F^{eq}] \quad (14)$$

where M^{-1} is the inverse of the transformation matrix M and f^* is the post collision distribution function in the population space. The shear kinematic viscosity ν is calculated by Eq. (5) and the bulk kinematic viscosity is calculated by $\eta = \left(\frac{1}{s_1} - \frac{1}{2}\right)c_s^2\delta_i - \frac{\nu}{3}$.

The MRT streaming step is executed in a similar fashion by Eq. (7) and the macroscopic velocity and density are computed by Eq. (8) & (9).

III. SIMULATION AND DISCUSSION

In the following simulations, basic flows which are used extensively in investigating variety of fluid flow problems, are simulated by the SRT and MRT methods, in two-

dimensional domains (2D). This is to highlight the strength and weakness of each of these methods.

Analysis of simple shear flow, uniaxial extensional flow and flow between two parallel plates under two different boundary conditions (fixed inlet velocity with the extrapolation method and pressure gradient) will be presented to expose the difference in the outcome of the SRT and the MRT methods. The simulated velocity profiles deviation from their corresponding theoretical solutions, will be used as indicators of the accuracy of either one of these two methods.

A. Simple shear flow

The domain size used in the subsequent simulations is basically a square $125 \times 125 \text{ lu}^2$ unless specified, with a top wall velocity range $U = 10^{-3} - 10^{-1} [\text{lu} \times \text{ts}^{-1}]$ and with similar magnitudes but negative sign at the lower wall. The unit [lu] stands for lattice space unit and [ts] for lattice timestep. The relaxation times used in the simulations were set to $\tau = 0.5263$ and $\tau = 40$, for two limiting cases. This led to kinematic viscosity $\nu = 0.008772 [\text{lu}^2 \times \text{ts}^{-1}]$ and $\nu = 13.167 \text{ lu}^2 \times \text{ts}^{-1}$ for the two cases, respectively. The density used in both cases was $\rho = 2 [\text{lm} \times \text{lu}^{-3}]$. The periodic boundary condition was imposed on the horizontal inlet and outlet surfaces. The velocity profile for Couette flows is given by:

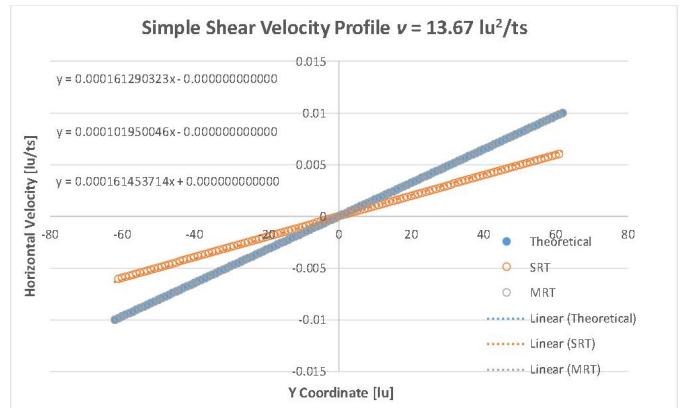
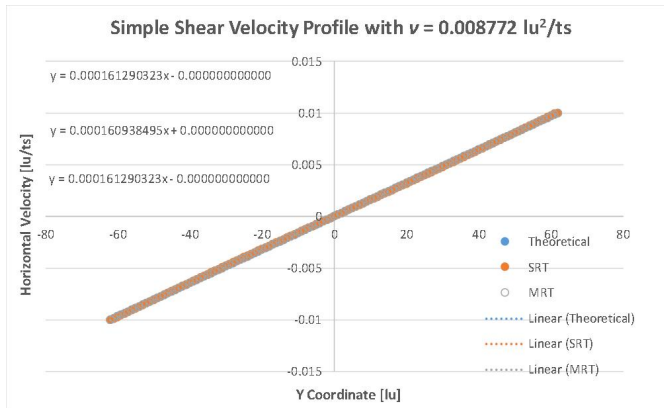


Fig. 2. Left: Simple shear flow profiles for low viscosity flows using the SRT and MRT methods. Right: simple shear flow profiles for high viscosity flows using the SRT and MRT methods. Both graphs display the linear curve fit equations for all conditions.

$$\frac{u}{U} = \frac{y}{b} - \frac{b^2}{2\mu U} \frac{\partial p}{\partial x} \left(\frac{y}{b}\right) \left(1 - \frac{y}{b}\right) \quad (15)$$

For simple shear flow characterized by zero pressure gradient in the horizontal direction, the equation simplifies to:

$$\frac{u}{U} = \frac{y}{b} \quad (16)$$

The velocity profile dependency on the viscosity of the fluid, shear strain rate and domain height are analyzed here. The comparison is executed by calculating the absolute relative error from the slopes of the curve fitted SRT and MRT simulation results S_s , S_m and the slope of the theoretical solution S_T . These slopes are constant since the simulated fluids are Newtonian.

As shown in the left section of Fig. 2, which depicts the low viscosity fluids with wall velocity $U = 10^{-2} [\text{lu} \times \text{ts}^{-1}]$,

both the SRT and the MRT methods produce reasonable results with absolute relative errors

$$\varepsilon_{slope,srt} = \text{abs}\left(\frac{(S_T - S_s)}{S_T}\right) = 0.0121 \quad \text{and}$$

$$\varepsilon_{slope,mrt} = \text{abs}\left(\frac{(S_T - S_m)}{S_T}\right) = 0.0099 \quad \text{for the SRT and MRT}$$

methods, respectively. The results shown in the right section of Fig. 2 for the high viscosity fluids, show a discrepancy in the outcome of the SRT method and a velocity jump at the wall, while the MRT method produces very accurate results. The following absolute relative errors $\varepsilon_{slope,srt} = 0.3679$ and

$\varepsilon_{slope,mrt} = 0.001$ are reported for the SRT and MRT methods,

respectively.

The inverse of the relaxation time used for the light viscosity fluid was $\omega_l = 1.9$ and the inverse of the relaxation time used for the high viscosity fluid was $\omega_h = 0.025$. The relaxation parameters used for the simulation of the low and high viscosity cases are $s_1 = 1.6$, $s_2 = 1.8$, $s_4 = s_6 = 8 \times \frac{(2-\omega)}{(8-\omega)}$.

In the next simulations the wall velocity was varied in the $125 \times 125 \text{ lu}^2$ domain such that, the shear strain rate changed from $\dot{\gamma} = 1.613 \times 10^{-3} \text{ ts}^{-1}$ to $\dot{\gamma} = 1.613 \times 10^{-5} \text{ ts}^{-1}$. With the low viscosity fluid, the MRT method shows some discrepancies close to the walls with high shear strain rate, while the SRT does not exhibit any dependency on the shear strain rate. No issues are recorded for the same cases with the low shear strain rates. The following absolute relative errors $\varepsilon_{\text{slope,srt}} = 0.0066$ and $\varepsilon_{\text{slope,mrt}} = 0.0768$ are reported for the high $\dot{\gamma}$ with low viscosity fluid, while absolute relative errors $\varepsilon_{\text{slope,srt}} = 0.0226$ and $\varepsilon_{\text{slope,mrt}} = 0.0219$ are calculated for the low $\dot{\gamma}$ with low viscosity fluid. The high viscosity cases resulted in relative errors $\varepsilon_{\text{slope,srt}} = 0.3679$ for the high and low $\dot{\gamma}$ by the SRT method, while relative errors

$\varepsilon_{\text{slope,mrt}} = 0.0046$ and $\varepsilon_{\text{slope,mrt}} = 0.0011$ are recorded for the high viscosity cases with the low and high $\dot{\gamma}$, respectively.

The discussion of Ginzbourg & Adler [27] about the influence of the domain height, on the error of the LBM solution for Poiseuille flow, indicated that the error was of the same order of $\frac{1}{z}$, where z was the domain height. This motivated the need for exploring the domain height's influence on the SRT solution in the subsequent simulations. The main weakness of the SRT method is observed as a jump in the velocity near the wall boundaries in high viscosity fluid flows. In the next simulations, the domain height was changed within a range of 200–3300 lu . The shear strain rate was maintained at $\dot{\gamma} = 1.613 \times 10^{-4} \text{ ts}^{-1}$.

TABLE I: THE SLOPES' ABSOLUTE RELATIVE ERRORS AS A FUNCTION OF THE DOMAIN HEIGHT

Domain Heights	200	300	600	1400	3300
$\varepsilon_{\text{slope,srt}}$	0.2723	0.2023	0.114	0.054	0.0383
$\varepsilon_{\text{slope,mrt}}$	0.001	0.001	0.0007	0.0178	0.0275

The results shown in the Table I, indicate a diminishing trend in the slopes' relative error of the SRT with the increase in domain height, meanwhile the MRT is indifferent to the changes in domain height.

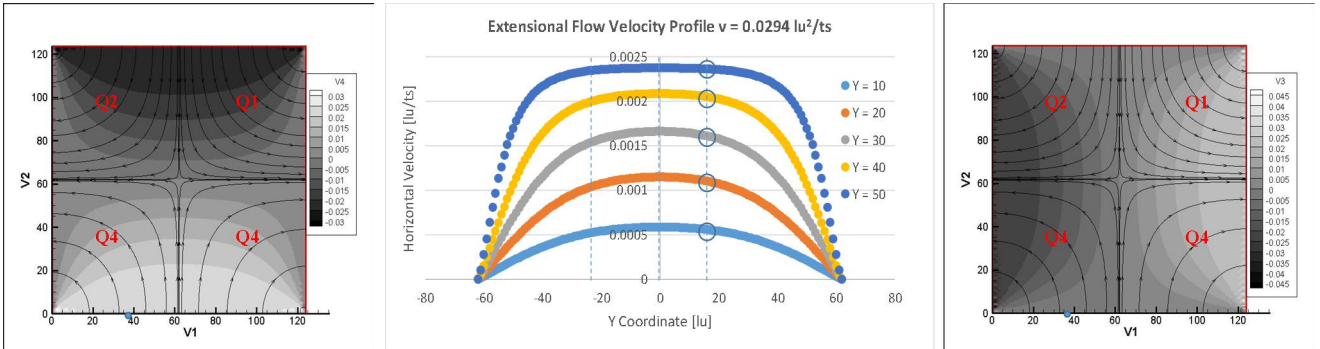


Fig. 3. Left: Extensional flow streamlines superimposed on the vertical velocity contours. Central top: horizontal velocity profiles in the first and fourth quadrant as function of the vertical coordinate at different horizontal positions. Right: extensional flow streamlines superimposed on the horizontal velocity contours.

B. Uniaxial Extensional Flow

Uniaxial extensional flows are used in variety of industrial applications. In uniaxial extensional flows, the fluid is sucked out of the domain in one direction (horizontal in the current simulation). The top and bottom boundaries are set as fluid sources where the flow is pulled in the vertical direction with the same inlet velocity magnitude for conserving the mass flow rate. The uniaxial extensional flow is imposed in 2D domains by applying a constant shear strain rate as follows:

$$\mathbf{u}^\infty(\mathbf{x}) = \dot{\gamma} \begin{pmatrix} 1 & 0 \\ 0 & -1 \end{pmatrix} \cdot \mathbf{x} \quad (17)$$

A domain size consisting of $125 \times 125 \text{ lu}^2$ was used, with shear strain rate range $\dot{\gamma} = \pm 4.03 \times 10^{-6} - 4.03 \times 10^{-4} [\text{ts}^{-1}]$ acting on the left and right horizontal boundaries. The relaxation times used in the simulations, were

$\tau = 0.58823$ and $\tau = 40$, leading to kinematic viscosity $\nu = 0.02914 \text{ lu}^2 \times \text{ts}^{-1}$ and $\nu = 13.167 \text{ lu}^2 \times \text{ts}^{-1}$, respectively. The density used in both cases was set to $\rho = 2 \text{ lmu} \times \text{lu}^{-3}$.

In Fig. 3, the left section shows the flow streamlines superimposed on the vertical velocity contour in gray scale and the right section depicts the flow streamlines superimposed on the horizontal velocity contours. The central part shows the horizontal velocity u_x as a function of the y vertical coordinate at different positions in the horizontal direction. It is worth noting that theoretically at any constant vertical position, curve fitting of the horizontal velocity magnitudes shown in blue circles, should yield a linear relationship with a slope equals to $\dot{\gamma}$. However, it is much easier to judge the accuracy of the SRT and MRT methods in uniaxial extensional flows, by assessing the conservation of mass at the inlet and outlet boundaries of the

domain. This is to be complemented by checking the symmetry of the horizontal velocity profile (mirror image) between the first and fourth quadrant and second and third quadrant at a horizontal location in the domain, which was selected arbitrarily as $x = 115[lu]$.

The velocity profile dependency on the viscosity of the fluid, shear strain rate and domain's height are reviewed in the subsequent simulations. A constant shear strain rate $\dot{\gamma} = \pm 4.03 \times 10^{-5} [ts^{-1}]$ was imposed on the left and right boundaries. For the high viscosity cases, the SRT velocity exhibits two jumps, while the MRT show a much smoother behavior. However, the results are almost identical for the low viscosity cases. The mass flow rate through the horizontal boundary is designated by \dot{m}_x , while the mass flow rate through the vertical boundary is designated by \dot{m}_y . The mass flow rate absolute relative error is calculated by

$$\varepsilon_{mfr} = abs \left(\frac{(\dot{m}_x - \dot{m}_y)}{\dot{m}_x} \right). \text{ The following relative errors}$$

$\varepsilon_{mfr,srt} = 0.00511$ and $\varepsilon_{mfr,mrt} = 0.00346$ are recorded for the low viscosity cases with the SRT and MRT methods, respectively. The high viscosity cases calculation yields absolute relative errors $\varepsilon_{mfr,srt} = 0.00772$ for the SRT method and $\varepsilon_{mfr,mrt} = 0.00531$ for the MRT method. Therefore, beside eliminating the velocity jumps, the MRT method can slightly improve the mass conservation of flows with high viscosity. The inverse of the relaxation time for the light viscosity fluid is $\omega_l = 1.7$ and for the high viscosity fluid is $\omega_h = 0.025$. The relaxation parameters used for the simulations of both high and low viscosity cases are $s_1 = 1.2$, $s_2 = 1.2$, $s_4 = s_6 = 8 \times \frac{(2-\omega)}{(8-\omega)}$.

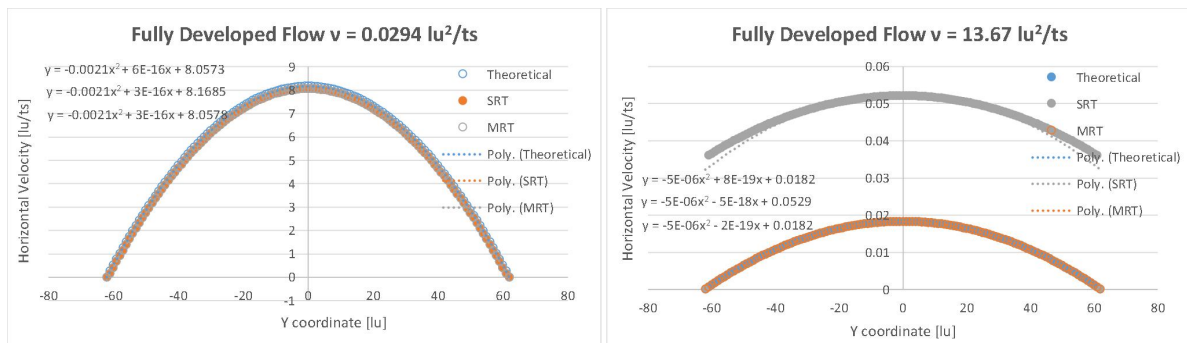


Fig. 4. Left: horizontal velocity profile for both the SRT and MRT methods for the low viscosity cases. Both methods yield results which match very well the theoretical profile. Right: horizontal velocity profile for flow between two parallel plates for the high viscosity flow.

The next two simulations were executed with the same domain size, high viscosity $\nu = 13.167 lu^2 \times ts^{-1}$ and two different shear strain rates $\dot{\gamma} = \pm 4.03 \times 10^{-6} [ts^{-1}]$ and $\dot{\gamma} = \pm 4.03 \times 10^{-4} [ts^{-1}]$. The two high viscosity cases with the MRT method, have the following absolute relative errors $\varepsilon_{mfr,lsr} = 0.0076$ and $\varepsilon_{mfr,hlsr} = 0.04$, which indicates a deterioration in the accuracy as the shear strain rate increases. However, the MRT method can eliminate the velocity jumps irrespective of the shear strain rate values used in the simulation

Several cases were executed with kinematic viscosity $\nu = 13.167 lu^2 \times ts^{-1}$ and multiple shear strain rate with a range of $\dot{\gamma} = \pm 4.03 \times 10^{-5} [ts^{-1}]$ and increased domain height from $H = 125[lu]$ to $H = 200[lu]$. The domain height does not improve the solution in uniaxial extensional flows with the SRT method.

C. Flow between Two Parallel Plates: Fully Developed Flow

Flow between two parallel plates are commonly used in variety of simulation cases. The velocity profile for flows between two parallel plates with constant source term is described by:

$$u = \frac{1}{2\mu} \frac{\partial p}{\partial x} (y^2 - h^2) \quad (18)$$

where $\frac{\partial p}{\partial x}$ is the pressure drop per unit length, μ is the dynamic viscosity of the fluid and h is half of the domain's height. The domain was a square $125 \times 125 lu^2$ unless specified. Two limiting cases with kinematic viscosities $\nu = 13.167 lu^2 \times ts^{-1}$ and $\nu = 0.0294 lu^2 \times ts^{-1}$ were applied. The density of the fluid was set to $\rho = 2.0 lmu \times lu^{-3}$. The periodic boundary condition was used for inlet and outlet surfaces along with the second order accurate bounce back condition on the bottom and top walls. The velocity profile dependency on the viscosity, source term and domain height for the flow between two parallel plates are analyzed here. The source term for imposing the pressure drop per unit length was set to $\frac{\Delta p}{\ell} = 2.5 \times 10^{-4}$ in the following simulations.

The graphs in the left section of Fig. 4, show that for the cases of low viscosity both methods yield reasonable results when compared with the theoretical solution and their velocity profiles conform with the theory. Meanwhile the SRT method's results for the high viscosity case in the right section of the figure, indicate a velocity jump at the wall and the velocity profile exhibits large deviation from the theoretical solution. On the contrary the MRT shows very good match with the theoretical solution for the high viscosity case. The error in the solution is assessed by using

the central velocities in the calculation of the absolute relative error. The high viscosity cases have the following absolute relative errors $\varepsilon_{y=0,srt} = 1.9$ for the SRT method and $\varepsilon_{y=0,mrt} = 0.0$ for the MRT method. While absolute relative errors $\varepsilon_{y=0,srt} = 0.0138$ and $\varepsilon_{y=0,mrt} = 7.4 \times 10^{-5}$ are reported for the low viscosity cases with the SRT and MRT methods, respectively. The inverse of the relaxation time for the light viscosity fluid is $\omega_l = 1.7$ and the same for the high viscosity fluid is $\omega_h = 0.025$. The appropriate relaxation parameters for the simulation of the low viscosity MRT case were found iteratively, and are reported as $s_1 = 1.7$, $s_2 = 1.6$, $s_4 = s_6 = 1.8$, while the suitable parameters for the simulation of the high viscosity case are given by $s_1 = s_2 = 0.6$, $s_4 = 1.8$, $s_6 = 0.4$.

The case with the high viscosity $\nu = 13.167 \text{ lu}^2 \times \text{ts}^{-1}$ was executed twice again with two different source terms $\frac{\Delta p}{\ell} = 2.5 \times 10^{-3}$ and $\frac{\Delta p}{\ell} = 2.5 \times 10^{-5}$ to check the influence of the source term on the MRT method's accuracy, in flows between two parallel plates. The absolute relative errors for the high source term are $\varepsilon_{y=0,mrt} = 1.63 \times 10^{-3}$ and $\varepsilon_{y=0,mrt} = 0.0$ for the low source term. This indicates that the MRT accuracy increases with the decrease in the value of the source term.

Several SRT cases were executed with a kinematic viscosity $\nu = 13.167 \text{ lu}^2 \times \text{ts}^{-1}$ and a source term $\frac{\Delta p}{\ell} = 2.5 \times 10^{-4}$ but the domain height was increased up to $h = \pm 4000 [\text{lu}]$. The results indicate that increasing the domain height improves the SRT solutions. Absolute relative errors $\varepsilon_{125,srt} = 2.376$, $\varepsilon_{4001,srt} = 0.0308$ and $\varepsilon_{8001,srt} = 0.0012$ are recorded for the three simulation cases with the SRT method. Increasing the domain height has a very profound influence on the results of the simulations for flows between two parallel plates.

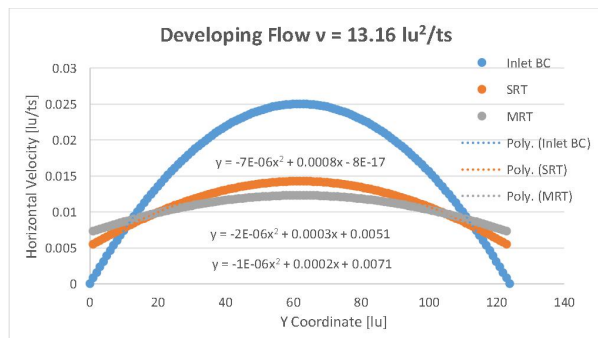
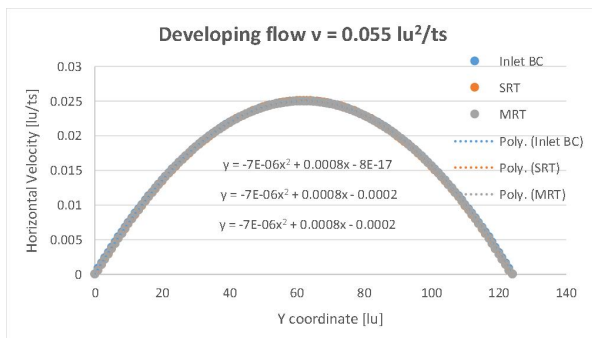


Fig. 5. Left: velocity profile comparison of the MRT and SRT at the outlet boundary with respect to the inlet boundary for the low viscosity cases. Right: velocity profile comparison of the MRT and SRT at the outlet boundary with respect to the inlet boundary for the high viscosity cases.

The same conditions from the previous simulations were used again. However, the inlet boundary central velocity was changed to $U_c = 2.5 \times 10^{-3} \text{ lu/ts}$ in one run and to $U_c = 1.5 \times 10^{-1} \text{ lu/ts}$ in the second. The kinematic viscosity

D. Flow between Two Parallel Plates: Developing Flow

Developing flows are achieved by applying a parabolic velocity boundary at the inlet of the simulation domain and treating the outlet boundary with the first or second order extrapolation method. The top and bottom wall conditions are imposed by using the second order bounce back method. The parabolic flow at the inlet boundary is imposed by using the following equation:

$$U_{(0,y,t)} = \frac{4U_{(0,\frac{H}{2},t)}y(H-y)}{H^2} \quad (19)$$

The velocity profile dependency on the fluid viscosity, the inlet boundary velocity and the domain's height of the developing flow behavior are analyzed here. The flow velocity profile in the subsequent simulations is tracked by comparing the profile at the outlet boundary to that of the inlet boundary condition, which is indicative of the transformation of the flow from developing to fully developed flow after achieving steady state condition. The domain is $125 \times 125 \text{ lu}^2$ and the inlet boundary has a parabolic velocity profile with central velocity $U_c = 2.5 \times 10^{-2} \text{ lu/ts}$. Two limiting cases characterized by $\nu = 0.055 \text{ lu}^2 \times \text{ts}^{-1}$ and $\nu = 13.167 \text{ lu}^2 \times \text{ts}^{-1}$ are presented in Fig. 5. The curves in the figure indicate that both SRT and MRT fail to achieve the condition of fully developed flow for the high viscosity case, and they both exhibit velocity jump near the wall. The cases with the low viscosity from both the MRT and SRT methods, show a very good match between the inlet velocity profile and the outlet velocity at the exit boundary. This indicates that fully developed flow condition is achieved.

The central velocity deficit expressed by $\zeta = \text{abs}\left(1 - \frac{U_{c,outlet}}{U_{c,inlet}}\right) \times 100$ is used to assess the performance of the two methods. The following deficits are reported for the light viscosity SRT and MRT cases, as well as for the heavy viscosity SRT and MRT cases as $\zeta_{lv,srt} = 0.1\%$, $\zeta_{lv,mrt} = 0.23\%$, $\zeta_{hv,srt} = 43\%$ and $\zeta_{hv,mrt} = 50.8\%$.

$\nu = 0.055 \text{ lu}^2 \times \text{ts}^{-1}$ was maintained in both simulations. The results indicate that the change in the central velocity magnitude influences moderately the accuracy of the results from both the SRT and MRT methods for the low viscosity cases. The central velocity deficit for the two cases with low

velocity are reported as $\zeta_{hvel,srt} = 0.52\%$, $\zeta_{hvel,srt} = 0.52\%$ and $\zeta_{hvel,srt} = 0.046\%$, $\zeta_{hvel,mrt} = 0.061\%$ are found for the high velocity cases. The relaxation parameters used for all the above MRT cases are $s_1 = 1.6$, $s_2 = 1.6$, $s_4 = s_6 = 0.5$, but the case of the higher velocity with $U = 0.15 lu/ts$, required the following relaxation parameters: $s_1 = s_2 = 0.3$, $s_4 = 1.0$, $s_6 = 0.9$. Two runs with inlet boundary central velocity set to $U_c = 2.5 \times 10^{-2} lu/ts$ and kinematic viscosity $\nu = 13. lu^2 \times ts^{-1}$ were used for investigating the domain height effects on the accuracy of the SRT and MRT method. Multiple domain heights were investigated between $H = 200 [lu]$ and $H = 3800 [lu]$. Both the MRT methods can match the theoretical velocity profile with the increase in the domain height. The central velocity deficit for the two cases are $\zeta_{200,srt} = 25.83\%$ and $\zeta_{200,mrt} = 30.75\%$ for the lower domain height and $\zeta_{3800,srt} = 0.036\%$, $\zeta_{3800,mrt} = 0.032\%$ for the increased domain height velocity.

IV. FLOW AROUND S822 AIRFOIL

In developing flow simulations, the MRT is not superior to the SRT, since it does not offer an improved solution for fluids with high viscosity. Meanwhile the SRT matches the MRT accuracy for fluids with low viscosity, however, the basic advantage of the MRT scheme is due to its capability of simulating flows with high Reynolds number. Unlike the SRT scheme which is capped by a relaxation time $\tau = 0.562$ for flows between two parallel plates, the MRT offers the opportunity to use a relaxation time as low

as $\tau = 0.50075$.

In the following the MRT is used for analyzing the flow around S822 airfoil. The LBM presents an opportunity for simulating such a complex phenomenon via a simplistic approach. It is well known that the LBM offers a computationally cheap and reasonably accurate second order bounce-back boundary condition. The bounce back is used on the upper, the lower walls and on the external surface of the foil in a 2D domain. Domain size $4500 \times 1000 lu^2$ was used to simulate the test portion of an airfoil wind tunnel as described in [23]. To achieve a reasonable fine mesh the cord length was set to $c = 1000 lu$, which was used as the reference length. The parabolic inlet velocity boundary was imposed by using a central velocity $U_c = 1.0 \times 10^{-2} lu/ts$. The central velocity was divided by the reference length to get an inverse of the reference time $\dot{\gamma}_{ref} = 1.0 \times 10^{-5} ts^{-1}$. The cord's Reynolds number for the simulation was calculated as $Re = 39,940$.

The foil lift and drag forces are calculated by the following formulae:

$$F_L = - \int_S (\mu \frac{\partial v_t}{\partial n} n_x + P n_y) dS \quad (20)$$

$$F_D = \int_S (\mu \frac{\partial v_t}{\partial n} n_y - P n_x) dS$$

where F_L is the lift force, F_D the drag force, μ is the fluid dynamic viscosity, P is the local pressure, v_t is the tangential velocity, and n_x, n_y are the x and y components of the normal to the contour of the foil S . The shear stress influence is included in the simulation, although its contribution is very marginal at such high Reynolds number. A phase field function is used to identify the foil external surface and it is calculated as follows:

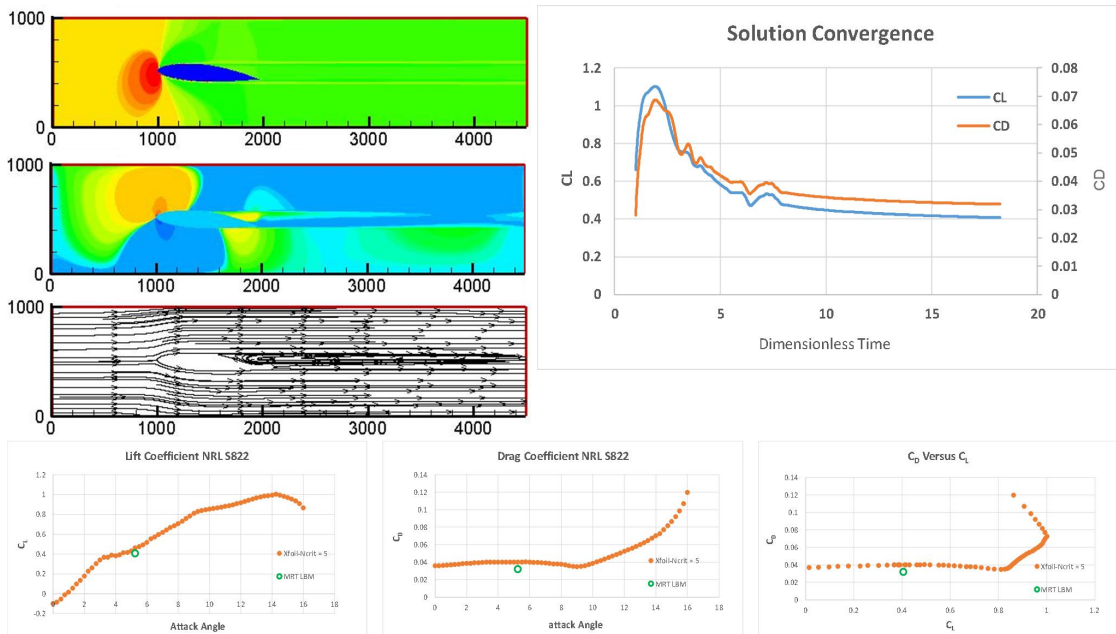


Fig. 6. Left top: pressure contour, vertical velocity contour and streamlines for flow around S822 airfoil with $Re = 39,940$ and 5.25 degrees angle of attack. Right top: streamlines for flow around S822 airfoil for the same conditions. Right top: lift and drag coefficients as a function of dimensionless time. Left bottom: MRT lift coefficient comparison with Xfoil results and turbulence amplification factor Nerit = 5. Center bottom: MRT drag coefficient comparison with Xfoil results and Nerit = 5. Right bottom: MRT drag versus lift coefficients comparison with Xfoil results and Nerit = 5.

$$\rho^N_{(x,t)} = \frac{\rho_{(x,t)}}{\rho_{(x,t)}} \quad (21)$$

where, $\rho_{(x,t)}$ is the fluid local density. This leads to $\rho^N_{(x,t)} = 1.0$ in the fluid domain, while the boundary nodes are assigned with $\rho^N_{(x,t)} = 0.0$ to enable the calculation of the phase field gradient $\nabla\rho^N$ which is used to track the solid boundary and to execute the calculation of the normal to the surface by: $\mathbf{n} = -\frac{\nabla\rho^N}{|\nabla\rho^N|}$

The vertical n_y and horizontal n_x components of the normal vectors are used in the calculation of the tangential velocity used in Eq. (20) for finding the lift and drag forces. The components of the tangential velocity are computed by the following:

$$\begin{aligned} u_{tx} &= u_x - n_x^2 u_x - n_x n_y u_y \\ u_{ty} &= u_y - n_y^2 u_y - n_x n_y u_x \end{aligned} \quad (22)$$

The derivative of the tangential velocity from Eq. (22) is calculated by the two points backward scheme at the fluid nodes adjacent to the foil surfaces, where the difference is $dv_i = v_i$, while the step in the normal direction is calculated by $dn = \text{abs}(n_y^{-1})$.

The one-third Simpson method is used to calculate the integrals for the lift and drag forces as follows:

$$I = \int_a^b I(x) dx \approx \frac{h}{3} \left[I(a) + 4 \sum_{i=2,4,6,\dots}^N I(x_i) + 2 \sum_{j=3,5,7,\dots}^{N-1} I(x_j) + I(b) \right] \quad (23)$$

where, the step in the integral is estimated by $h = \frac{S}{C}$ and C is determined by setting a counter for the number of foil boundary nodes, which constitute the external contour of the foil. The length of the foil is calculated by: $S \approx \int_a^b \sqrt{1 + [f'(x)]^2} dx$.

where, $f(x)$ is the foil set of shape equations used to create the foil geometry in the 2D domain.

The drag and lift coefficients are calculated by the following equations:

$$\begin{aligned} C_L &= \frac{2F_L}{\rho\bar{U}^2 D} \\ C_D &= \frac{2F_D}{\rho\bar{U}^2 D} \end{aligned} \quad (24)$$

The pressure contour, the horizontal velocity contour and the streamlines of the flow around NRL S822 airfoil with 5.250 attack angle, bounded by top and bottom walls as is the situation in a wind tunnel testing, are shown in the top left part of Fig. 6. The right top section of the figure illustrates the lift and drag coefficients evolution with respect to a dimensionless time as an indication of the solution convergence. The bottom left side of the figure shows the MRT solution for the lift coefficient as compared to XFOil's outcome [24], which is usually used for guidance

in airfoil wind tunnel testing [25]. The bottom center of the figure shows the MRT solution for the drag coefficient and the bottom right is the drag coefficient as a function of the lift coefficient, in comparison with the XFOil solution.

The presented results of the simulations in Fig. 6 were achieved at a dimensionless time step $t_{ref} = 18.24$ with a convergence criterion $\varepsilon = 6.5 \times 10^{-8}$. The results show a reasonable agreement with the results of XFOil for the S822 airfoil with turbulence amplification factor $N_{crit} = 5$ and cord's Reynolds number $Re = 50,000$.

The relaxation parameters for the presented case are $s_1 = s_2 = 0.01$, $s_3 = 1.1$, $s_4 = 1.2$.

V. CONCLUSION

The Boltzmann MRT and SRT methods are used in basic fluids flow simulations for delineating the advantages and disadvantages of both methods. It was shown that there are wide variety of flow conditions where the SRT method can be used successfully, and that even though the MRT is very powerful, it fails in overcoming all the shortfalls of the SRT methods.

For simple shear flow, the MRT can always eliminate the velocity jump at the walls exhibited by the SRT for fluid flows characterized by high viscosity. The MRT, however shows some inaccuracy at the walls for simulations involving low viscosity fluids and high shear strain rate. In the simulation of simple shear flow with the use of the SRT method, the domain height can eliminate the velocity jump at the walls under all conditions. While the SRT can accurately describe fluids flow with low to moderate viscosities.

For uniaxial extensional flow, the MRT method show superiority over the SRT at all levels. The domain height in the SRT method cannot be used for correcting the velocity field in this type of flows. The SRT method is generally accurate for low to moderate viscosity fluids subjected to extensional flow conditions.

For fully developed flows between two parallel plates, the MRT excels in providing accurate results for high viscosity flows under variety of source terms. The domain height in the SRT method can be used for eliminating the inaccuracy of the results for high viscosity fluid flows.

For developing flow between two parallel plates, the MRT does not show any advantage over the SRT method for cases with high viscosity fluids. Meanwhile the domain height has a major influence on the accuracy of the results for both MRT and SRT methods. In general, the SRT method is accurate for simulating low to moderate viscosity fluids, although high central velocities can moderately deteriorate the results. The main advantage of the MRT over the SRT method is due to its capability to simulate flows with ultra-low fluid viscosity, and hence large Reynolds numbers as this was shown in the simulation of flow around S822 airfoil.

CONFLICT OF INTEREST

The authors declare no conflict of interest.

AUTHOR CONTRIBUTIONS

Wessam F. Hasan: developed the base MRT model.

Ameer K. Alhilo: wrote the module for the lift and drag coefficient calculations, ran the simulation and analysis and wrote the paper.

Hassan Farhat: defined the content and designed the simulation cases, supervised the code writing, edited and proof read the manuscript.

ACKNOWLEDGMENT

The authors like to thank The Higher Committee for Education Development in Iraq (HCED) for their financial support.

REFERENCES

[1] D. D'Humieres, "Generalized lattice Boltzmann equation," *Rarefied Gas Dynamics: Theory and Simulations, Progress in Astronautics and Aeronautics*, vol. 159, 1992, pp. 45-458.

[2] L. Pierre and L.-S. Luo, "Theory of the lattice Boltzmann method: Dispersion, dissipation, isotropy, Galilean invariance, and stability," *Physical Review E*, vol. 61, no. 6, p. 6546, 2000.

[3] D. D'Humieres, "Multiple-relaxation-time lattice Boltzmann models in three dimensions," *Philosophical Transactions of the Royal Society of London. Series A: Mathematical, Physical and Engineering Sciences*, vol. 360, no. 1792, pp. 437-451, 2002.

[4] J. S. Wu and Y. L. Shao, "Assessment of SRT and MRT scheme in parallel lattice Boltzmann method for lid-driven cavity flows," in *Proc. The 10th National Computational Fluid Dynamics Conf.*, 2002.

[5] D. Rui, B. C. Shi, and X. W. Chen, "Multi-relaxation-time lattice Boltzmann model for incompressible flow," *Physics Letters A*, vol. 359, no. 6, pp. 564-572, 2006.

[6] Z. L. Guo, B. C. Shi, and N. C. Wang, "Lattice BGK model for incompressible Navier-Stokes equation," *Journal of Computational Physics*, vol. 165, no. 1, pp. 288-306, 2000.

[7] J. Saeed and M. Rahnama, "Shear-improved Smagorinsky modeling of turbulent channel flow using generalized Lattice Boltzmann equation," *International Journal for Numerical Methods in Fluids*, vol. 67, no. 6, pp. 700-712, 2011.

[8] E. Aslan, I. Taymaz, and A. C. Benim, "Investigation of the lattice Boltzmann SRT and MRT stability for lid driven cavity flow," *International Journal of Materials, Mechanics and Manufacturing*, vol. 2, no. 4, pp. 317-324, 2014.

[9] S. Kazuhiko *et al.*, "A D3Q27 multiple-relaxation-time lattice Boltzmann method for turbulent flows," *Computers & Mathematics with Applications*, vol. 69, no. 6, pp. 518-529, 2015.

[10] B. Younes and A. Omidvar, "Calculation of friction coefficient and analysis of fluid flow in a stepped micro-channel for wide range of Knudsen number using Lattice Boltzmann (MRT) method," *Physica A: Statistical Mechanics and its Applications*, vol. 440, pp. 161-175, 2015.

[11] L. Dong, Z.-X. Tong, Q. L. Ren, Y.-L. He, and W.-Q. Tao, "Three-dimensional lattice Boltzmann models for solid-liquid phase change," *International Journal of Heat and Mass Transfer*, vol. 115, pp. 1334-1347, 2017.

[12] K.-N. Hojjat and H. Niazmand, "A double MRT-LBM for simulation of mixing in an active micromixer with rotationally oscillating stirrer in high Peclet number flows," *International Journal of Heat and Mass Transfer*, vol. 122, pp. 913-921, 2018.

[13] H. Sajjadi, A. A. Delouei, M. Sheikholeslami, M. Atashafrooz, and S. Succi, "Simulation of three dimensional MHD natural convection using double MRT Lattice Boltzmann method," *Physica A: Statistical Mechanics and its Applications*, vol. 515, pp. 474-496, 2019.

[14] M. Jami, F. Moufekkir, A. Mezrhaj, J. P. Fontaine, and M. Bouzidi, "New thermal MRT lattice Boltzmann method for simulation of convective flows," *International Journal of Thermal Sciences*, vol. 100, 2016, p. 98e107.

[15] I. Taro, K. Suzuki, T. Nakamura, and M. Yoshida, "Flow simulation around an airfoil using lattice Boltzmann method on generalized

coordinates," in *Proc. 42nd AIAA Aerospace Sciences Meeting And Exhibit*, 2004, p. 244.

[16] I. Taro, K. Suzuki, T. Nakamura, and M. Yoshida, "Acceleration of steady-state lattice Boltzmann simulations on non-uniform mesh using local time step method," *Journal of Computational Physics*, vol. 202, no. 2, pp. 645-663, 2005.

[17] S. Rajani, Y. B. Li, R. Shock, and B. Duncan, "Computational analysis of a wingtip vortex in the near-field using LBM-VLES approach," in *Proc. 49th AIAA Aerospace Sciences Meeting including the New Horizons Forum and Aerospace Exposition*, 2011, p. 679.

[18] S. Rajani, Y. B. Li, R. Shock, and S. Noelting, "Unsteady flow analysis of a multi-element airfoil using lattice Boltzmann method," *AIAA Journal*, vol. 50, no. 9, pp. 1805-1816, 2012.

[19] X.-P. Chen, "Applications of lattice Boltzmann method to turbulent flow around two-dimensional airfoil," *Engineering Applications of Computational Fluid Mechanics*, vol. 6, no. 4, pp. 572-580, 2012.

[20] J. N. N. Council and K. G. Boulama, "Validating the URANS shear stress transport γ -Re θ model for low-Reynolds-number external aerodynamics," *International Journal for Numerical Methods in Fluids*, vol. 69, no. 8, pp. 1411-1432, 2012.

[21] P. Amin and M. Mirzaei, "Flow Simulation around cambered airfoil by using conformal mapping and intermediate domain in lattice Boltzmann method," *Journal of Statistical Physics*, vol. 166, no. 2, pp. 354-367, 2017.

[22] P. R. Prabhukhot and A. R. Prabhukhot, "Computer analysis of S822 aerofoil section for blades of small wind turbines at low wind speed," *Journal of Solar Energy Engineering*, vol. 139, no. 5, 2017.

[23] I. Ginzbourg and P. M. Adler, "Boundary flow condition analysis for the three-dimensional lattice Boltzmann model," *Journal de Physique II*, vol. 4, no. 2, pp. 91-214, 1994.

[24] M. Drela, "XFOIL: An Analysis and design system for low Reynolds number airfoils," *Lecture Notes in Engineering: Low Reynolds Number Aerodynamics*, vol. 54, Springer-Verlag, New York, June 1989.

[25] M. S. Selig, *Summary of Low Speed Airfoil Data*, vol. 1, SoarTech, 1995.

Copyright © 2020 by the authors. This is an open access article distributed under the Creative Commons Attribution License which permits unrestricted use, distribution, and reproduction in any medium, provided the original work is properly cited ([CC BY 4.0](https://creativecommons.org/licenses/by/4.0/)).



Ameer K. Alhilo is a Ph.D Candidate at Wayne state University Detroit Michigan, USA. His main research area is in thermal fluid simulation and renewable energy. He is a faculty member at Wasit University Kut Iraq.



Wessam F. Hasan is a PhD in mechanical engineering at Wayne State University, MI, USA. He has got the MSc in mechanical engineering from Wayne State University, MI, USA. Also, he got the MSc in mechanical engineering from University of Technology, Baghdad, Iraq. He is a mechanical engineer at North Oil Company, Kirkuk, Iraq.



Hassan Farhat got the MSc in mechanical engineering (internal combustion) from the Institute of Mech. & Elec. Engineering, Varna Bulgaria; MSc in mechanical engineering (thermal sciences) from Wayne State University, MI, USA. He also got the PhD in mechanical engineering from Wayne State University, MI, USA. His research area is in emulsions and interface physics.